Strong spin-lattice coupling and high-temperature magnetic ordering in monolayer chromium dichalcogenides

Strong spin-lattice coupling and high-temperature magnetic ordering in monolayer chromium dichalcogenides

A. González-García,[1,2] C. Bacaksiz,[2,3,4] T. Frauenheim,[4,5,6] and M. V. Milošević[2,7,*]

[1] *Grupo de Investigación en Física Aplicada, Departamento de Física, Universidad del Norte, Barranquilla, Colombia*
[2] *Department of Physics & NANOlab Center of Excellence, University of Antwerp, Groenenborgerlaan 171, 2020 Antwerp, Belgium*
[3] *Computational Biotechnology, RWTH Aachen University, Worringerweg 3, 52074 Aachen, Germany*
[4] *Bremen Center for Computational Material Science (BCCMS), Bremen D-28359, Germany*
[5] *Shenzhen JL Computational Science and Applied Research Institute, Shenzhen 518131, China*
[6] *Beijing Computational Science Research Center, Beijing 100193, China*
[7] *Instituto de Física, Universidade Federal de Mato Grosso, Cuiabá, Mato Grosso 78060-900, Brazil*

(Dated: July 10, 2024)

We detail the magnetic properties of monolayer CrX_2 and its Janus counterparts CrXY (X,Y=S,Se,Te, with X≠Y) using *ab initio* methods and Landau-Lifshitz-Gilbert magnetization dynamics, and uncover the pronouncedly strong interplay between their structure symmetry and the magnetic order. The relaxation of non-magnetic chalcogen atoms, that carry large spin-orbit coupling, changes the energetically preferential magnetic order between in-plane anti-ferromagnetic and tilted ferromagnetic one. The considered Janus monolayers exhibit sizeable Dzyaloshinskii-Moriya interaction, in some cases above 20% of the isotropic exchange, and critical temperature of the long-range magnetic order in the vicinity or even significantly above the room temperature.

PACS numbers:

I. INTRODUCTION

Most 2D materials are not magnetic in their pristine form. Thermal fluctuations suppress long-range magnetic order in monolayers at any non-zero temperature[1,2], unless that detrimental effect of fluctuations is neutralized by the presence of magnetic anisotropy, which can be induced in a 2D crystal by e.g. doping with transition metals[3–6]. The microscopic source of magnetic anisotropy is the spin-orbit coupling (SOC), which is sizeable in all the magnetic 2D materials realized to date, starting from the pioneering discoveries of long-range magnetism in monolayer CrI_3[7] and $CrGeTe_3$[8] (for a recent review, see[9]). When the spin-orbit coupling is combined with a broken spatial inversion symmetry, the Dzyaloshinskii-Moriya interaction (DMI) arises within the magnetic material[10,11]. DMI is an antisymmetric magnetic exchange interaction that orients the neighbouring spins orthogonally to each other, with a unique sense of rotation, instead of the (anti)parallel spin alignments stemming from the usual Heisenberg exchange interaction[12].

In parallel with the rise of 2D magnetic materials, recent years have witnessed the advent of Janus monolayers. Named after a two-faced god from Roman mythology, Janus 2D materials have different top and bottom surfaces, which breaks the mirror symmetry and instigates their unique physical, chemical, and quantum properties, promising for many potential applications[13–16]. Janus transition-metal dichalcogenide (JTMDC) monolayers (MXY, where M=Mo,W, X,Y=S,Se,Te, and X≠Y), have been theoretically found to be dynamically stable[15,17] and were experimentally synthesized[18,19]. Despite the strong Rashba SOC in these materials, long-range magnetism was not observed. Magnetic Janus 2D materials are expected to host strong intrinsic polarization and piezoelectric response, coupled to pronounced Dzyaloshinskii-Moriya interaction (DMI), which would recommend them for diverse multifunctional applications in spintronics, memory, logic and magnetoelectric devices. To date, 2D Janus $Cr_2Cl_3I_3$ has been reported to be a FM-semiconductor material with a direct band gap[20], and strong emergent DMI has been predicted in 2D Janus manganese dichalcogenides MnXY (X,Y=S,Se,Te, with X≠Y)[21,22], VSeTe[22] and $Cr(I,X)_3$ (X=Br,Cl)[23] by first-principles calculations[21]. Recently, two-dimensional Cr-based dichalcogenide halides CrYX (where Y = S, Se, Te; and X = Cl, Br, I), have demonstrated appealing multifunctional capabilities in the domain of topological electronic and valleytronic device applications[24].

Since monolayer 1T-CrS_2[25,26], $CrSe_2$[26–28] and $CrTe_2$[26,29–31] crystals have been successfully synthesized, and recently a room-temperature ferromagnetism has been found in 2D $CrTe_2$ films[31], the prospects of experimental realization of the magnetic Janus CrXY (X,Y=S,Se,Te, with X≠Y) are growing by the day. He *et al.* have theoretically investigated the physical properties of such chromium Janus dichalcogenides using first-principle methods[32]. However, the structural changes and the corresponding variety of the emergent magnetic interactions and possible non-collinear orderings were not considered, which calls for a more rigorous study. Therefore, motivated by above-mentioned developments and prospects, we here detail the structural, electronic and magnetic properties of 2D CrX_2 and their Janus counterpart CrXY monolayers (X,Y=S,Se,Te, with X≠Y) using relativistic density-functional calculations.

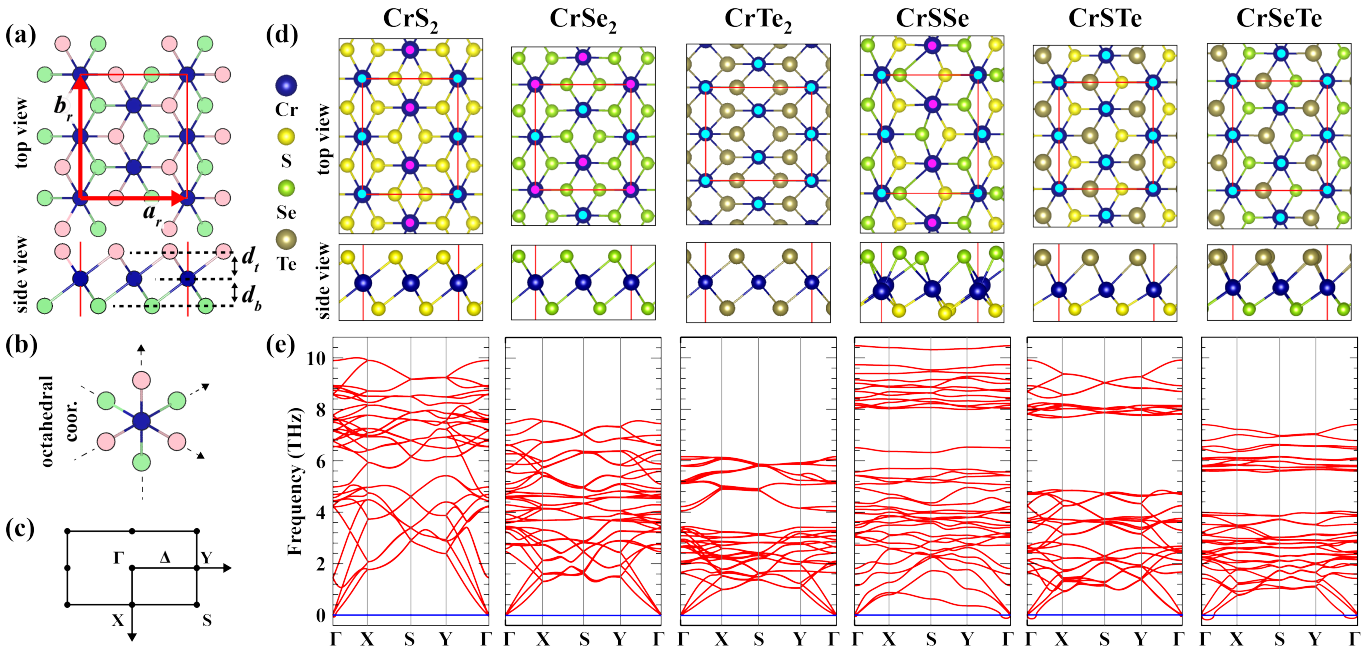

FIG. 1: Schematic representation for: (a) top view of the rectangular unit-cell for CrX_2 (X=S,Se,Te); blue atoms denote Cr, and green/pink ones show the chalcogen atoms (S, Se, Te) of bottom/top surface. $a_r(x)$ and $b_r(y)$ are the lattice vectors; d_t/d_b denote the distance between the Cr layer and top/bottom chalcogen layer. (b) Octahedral coordination of each Cr atom, and (c) top view of the high symmetry points in the Brillouin zone for the rectangular unit-cell of (J)TMDCs. (d) Top and side view of the considered TMDC and JTMDC systems, with atoms denoted by color as shown on the left. The individual magnetic moments of the ground-state magnetic order are shown on Cr atoms as purple (spin-down) and cyan dots (spin-up). (e) Phonon band structures of the monolayers shown in (d).

In doing so, we reveal the particularly strong spin-lattice coupling, high-temperature long-range magnetic order, and sizeable DMI, which in combination with polarization due to symmetry breaking makes these materials a uniquely versatile magneto-electronic playground worthy of further experimental effort.

II. COMPUTATIONAL DETAILS

The analysis of structural, phonon, electronic and magnetic properties of Cr-based TMDCs and JTMDCs was carried out using relativistic density-functional theory calculations[33,34]. Perdew–Burke–Ernzerhof functional[35] was used to treat the electron exchange-correlation interactions. The ion-electron interactions were described by the projector augmented wave (PAW) method[36,37], implemented in the Vienna ab-initio simulation package (VASP)[38,39]. For optimization of the lattice parameters, the electron wave-function was expanded in plane waves up to a cutoff energy of 700 eV, and a Γ-centered grid of 6×6×1 k-points was used to sample the irreducible Brillouin zone. The geometric convergence criterion for energy was set at 10^{-7} eV. Furthermore, Grimme's method (DFT-D2) was used to treat long-range electronic correlations[40]. Due to the possible existence of the polarization dipole in Janus CrXY monolayers, the dipole correction is taken into account. To avoid the periodic interactions, a 20 Å vacuum was kept as vertical spacing between the adjacent layer. The spin-orbit interaction (SOC) is fully considered. On-site Coulomb interactions of 3d-Cr orbitals were taken into account using DFT+U[41] approach. U parameters of each considered monolayer were obtained separately using a linear response method[42], as 3.72, 3.90, 3.79, 3.81, 3.75, and 3.84 eV for CrS_2, $CrSe_2$, $CrTe_2$, CrSSe, CrSTe and CrSeTe, respectively. In order to examine the dynamical stability of our systems, we have calculated the phonon dispersion using PHONOPY[43], based on the finite-displacement method (FDM)[44,45]. First-principles phonon calculations have been performed by taking into account the interactions in 3×3×1 supercells consisting of 36 Cr atoms and 72 chalcogen atoms. To obtain magnetic exchange interactions between Cr atoms, we employed the four-state energy mapping methodology (4SM)[46,47]. The magnetic ground state and the temperature-dependent magnetization were then calculated using the atomistic spin simulation code *Spirit*, based on the Landau–Lifshitz–Gilbert (LLG) formalism[48].

TABLE I: Calculated structural parameters of pristine and Janus Cr-dichalcogenide monolayers. $a_r(x)$ and $b_r(y)$ are the lattice vectors of the rectangular unit-cell. $n = \frac{a_r}{b_r}/\frac{\sqrt{3}}{2}$ illustrates the deviation of the lattice structure from the ideal triangular lattice. d_t and d_b are the respective distances of the Cr layer from the top and bottom chalcogen layers. Ratio d_t/d_b then reflects the vertical symmetry breaking in the structure. ρ_t and ρ_b are the charge transfers between the Cr and top and bottom chalcogen atom respectively. m, in units of Bohr magneton μ_B, is the on-site magnetic moment. MS is the lowest-energy magnetic configuration among the considered magnetic orders in the DFT scheme: $s-$, $z-$, $out-$, and $in-$ stand for *stripy*, $zig-zag$, $out-of-plane$, and $in-plane$, respectively. ES gives the electronic state, i.e. metallic (m) or semiconductor (s).

	a_r [Å]	b_r [Å]	n	d_t [Å]	d_b [Å]	d_t/d_b	ρ_t [e]	ρ_b [e]	m [μ_B]	MS	ES
CrS_2	5.51	6.67	0.95	1.49 (S)	1.49 (S)	1.00	0.59 (S)	0.59 (S)	2.5	$s-$AFM	m
$CrSe_2$	6.01	6.61	1.05	1.63 (Se)	1.63 (Se)	1.00	0.51 (Se)	0.51 (Se)	2.7	$z-$AFM	m
$CrTe_2$	7.32	6.42	1.32	1.78 (Te)	1.78 (Te)	1.00	0.42 (Te)	0.42 (Te)	3.2	$out-$FM	m
CrSSe	5.66	6.94	0.94	1.91 (Se)	1.32 (S)	1.45	0.43 (Se)	0.71 (S)	3.0	$s-$AFM	s
CrSTe	6.07	6.87	1.02	2.06 (Te)	1.24 (S)	1.66	0.36 (Te)	0.71 (S)	2.9	$out-$FM	m
CrSeTe	6.17	7.14	1.00	1.98 (Te)	1.42 (Se)	1.39	0.37 (Te)	0.59 (Se)	3.0	$in-$FM	m

III. RESULTS AND DISCUSSION

A. Structural and electronic properties

Pristine TMDC monolayers 1T-CrX_2 (X = S, Se, and Te) have the triangular lattice layer of Cr atoms sandwiched between the two triangular lattices of the chalcogen atoms in the A-B-C stacking, as shown in Fig. 1(a). Cr atom exhibits octahedral coordination (O_h, shown in Fig. 1(b)). As three different chalcogen atoms are considered in our study, the three different Janus CrXY monolayers were examined: CrSSe, CrSTe, and CrSeTe. In order to depict possible distortions and/or reconstructions, we consider a rectangular unit-cell with 4 Cr and 8 chalcogen atoms. The structural analyses of those six monolayer materials are done by including spin-orbit coupling and considering the ferromagnetic (FM), zig-zag anti-ferromagnetic ($z-$AFM), and stripy anti-ferromagnetic ($s-$AFM) states. While keeping the considered magnetic order fixed, the atomic positions as well as the lattice vectors of the structure were optimized, and the energies of all the possible magnetic states (with converged structure) were compared. In Table I, we list the so-obtained structural parameters and the corresponding lowest-energy magnetic states for each of the systems. Note that the shown and listed magnetic states are the lowest energy ones among the three considered magnetic orders. The structure with the lowest energy is used for magnetic exchange interaction calculations. The obtained magnetic exchange parameters are used in LLG spin simulations to determine the magnetic ground-state which are compared with the states listed in Table I. It is worth mentioning that among the six materials studied here, Janus CrSSe stands out due to several distinctive characteristics. Firstly, it exhibits notable changes in the structural depending on the magnetic order. Secondly, it is the only material exhibiting a semiconducting nature. Lastly, on the contrary to initial DFT analysis, it exhibits FM magnetic ground state achievable through the LLG scheme further in the investigation. Each of these aspects is discussed in detail in their respective sections.

As shown in Fig. 1, each material maintains triangular lattice and octahedral coordination of the Cr atoms. However, the in-plane symmetry is broken in each structure. In addition, the out-of-plane symmetry is broken for the Janus structures. In order to quantify in-plane asymmetry, we define a parameter $n = \frac{a_r}{b_r}/\frac{\sqrt{3}}{2}$ (the normalized ratio between lattice vectors, a_r/b_r, with respect to that of the perfect triangular lattice ($\sqrt{3}/2$)), and listed its values for the ground state of different materials in Table I. The lattice sizes increase with the size of the chalcogen atoms, as expected. The in-plane asymmetry parameter, n, on the other hand, also increases for the pristine structures. However, for the Janus ones, it changes slightly and remains close to 1, which is the value of the perfect triangular lattice. To reveal the interplay between the structure symmetry and the magnetic order even more clearly, in Table II we list the values of the in-plane asymmetry parameter of the pristine and Janus structures for different considered magnetic orders. All structures except $CrTe_2$ exhibit significant variation in parameter n with magnetic order, which demonstrates the *strong spin-lattice coupling in these compounds*. We will return to this important point again in the discussion

TABLE II: The in-plane asymmetry parameter, n, of the pristine and Janus structures of Cr-dichalcogenide monolayers with different magnetic orders. $n = \frac{a_r}{b_r}/\frac{\sqrt{3}}{2}$ (the normalized ratio between lattice vectors, a_r/b_r, with respect to that of the perfect triangular lattice ($\sqrt{3}/2$)).

	FM	$z-$AFM	$s-$AFM
CrS_2	1.00	1.02	0.95
$CrSe_2$	0.98	1.05	0.92
$CrTe_2$	1.32	1.29	1.30
CrSSe	0.99	1.05	0.94
CrSTe	1.02	0.94	0.92
CrSeTe	1.00	0.93	0.92

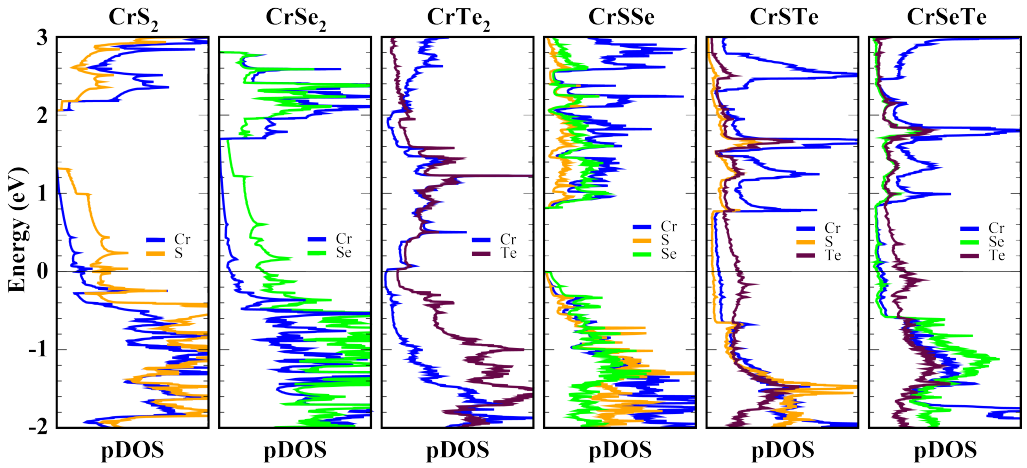

FIG. 2: Projected density of states (pDOS) of the Cr (blue), S (orange), Se (green) and Te (brown) atoms for the considered CrXY (X,Y=S,Se,Te) magnetic systems, calculated with SOC included. Fermi energy is set to 0 eV.

further down the article.

Another parameter that shows the structural changes is the out-of-plane asymmetry. In Table I, the distances between the Cr layer and the top or bottom chalcogen layer (d_t or d_b, respectively) and their ratios (d_t/d_b) are given. The pristine monolayers are symmetric in the out-of-plane direction. Those distances increase with increasing size of the involved chalcogen. Specifically, the distances between the layers of Cr and S atoms and Cr and Se atoms in CrS_2 and $CrSe_2$ are 1.49 and 1.63 Å, respectively. However, in the Janus CrSSe, the corresponding distances are 1.32 and 1.91 Å, respectively. Such a trend also exists in other layers and their Janus counterparts. In short, in Janus monolayers the Cr-chalcogen distance decreases (increases) compared to the pristine monolayer case when the chalcogen atom at the opposite side is larger (smaller). The most asymmetric case is CrSTe with $d_t/d_b = 1.66$. Our Bader charge analyses align with the behavior of the atomic layer distances (d_t and d_b). S, Se, and Te atoms accept $0.59e$, $0.51e$, and $0.42e$ from Cr atom in pristine monolayer cases, respectively. In general, the shorter bond length indicates the larger charge transfer. In the Janus cases, the charge transfer decreases (increases) when the chalcogen atom on the opposite side is larger (smaller). Similar trends for the lattice constant and the bond length were reported in earlier studies of 2D Janus monolayer structures[21,49]. As mentioned above, the Janus CrSSe particularly differs from the others due to the significantly distorted octahedral coordination of one of the Cr atoms alongside with the buckled form of the Cr layer, as seen in Fig. 1(d).

To validate the stability of the obtained structures, the vibrational (phonon) calculations were performed, with results shown in Fig. 1(e). In general, there are no imaginary frequencies in the phonon dispersion, except for weak deviations at around Γ point in some cases that are likely due to insufficiently large supercell (limited by the computational load). This feature has been found in other 2D Janus systems[17,50], is usually discarded as a technicality, and highlights the flexural acoustic mode of these materials. Moreover, since the 2D JTMDCs are synthesized on the substrate[17,18,50], any bending instability would be voided in reality. We thus conclude that the presented phonon dispersions validate the stability of each considered structure. The reduction of the frequency levels of the phonon bands as the size of the chalcogen atoms increases indicates that the bonds are also softening with the size of the atoms involved.

As mentioned above, our structural analysis shows that structural properties of the considered Cr-dichalcogenides strongly depend on the established magnetic order (be it FM, $z-$AFM, or $s-$AFM) and vice-versa. Considering the magnetic state shown in Fig. 1(d), the lattice tends to expand in the direction of ferromagnetically aligned chains while it is compressed in the direction of the antiferromagnetic chains. Such behavior is evident in all the AFM systems.

With regard to the reported electronic properties of the 1T-CrX_2 in the literature, all of them are observed metallic[27,31,51–55]. Indeed, in all our CrX_2 structures, a metallic character is found, as shown in Fig. 2. On the other hand, we found that 2D Janus CrSSe is an Y-Δ indirect semiconductor (see Fig. 2 and Fig. 1(c)), with a bandgap in the infrared electromagnetic spectrum (0.80 eV) and a direct (Y-Y) optical transition at 0.82 eV. This intrinsic ferromagnetic yet semiconducting nature of CrSSe, which is scarce in the literature, is interesting for potential applications in opto-spintronic nanodevices[56,57]. Conversely, our results show that both CrSTe and CrSeTe exhibit also exhibit ferromagnetic but metallic nature. This span of possibilities from ferromagnetic indirect/direct semiconductor to ferromagnetic metals among the 2D Janus CrXY systems, possibly highly prone to external stimuli, suggests these materials for potential applications in (multifunctional) magnetic nanodevices and sensors.

TABLE III: Calculated magnetic exchange interaction parameters: the isotropic exchange (the diagonal elements of the interaction matrix), J_{ij}^{xx}, J_{ij}^{yy} and J_{ij}^{zz}; the DMI vector components D_{ij}^{x}, D_{ij}^{y}, D_{ij}^{z}, and modulus $|D|$; the ratio between the DMI and the average isotropic interaction $|D|/\langle J_{ij}\rangle$; the magnetic moment m of Cr, in units of Bohr magneton μ_B; the critical temperature T_c; and the magnetic ground state (MGS) at $T = 0$ K. $s-$ and $z-$ indicate *stripy* and *zig-zag*, respectively. $in-xy$ means that the magnetic lowest energy on Cr atoms are pointing in xy plane (xy in-plane). $t-xyz$, $t-xz$ and $t-yz$ stand for tilted magnetic alignment in x, y, and z; x an z, and y and z, respectively. Nomenclature of the pairs (i,j) is shown in Fig. 3. The distance between the i and j atoms of (i,j) pairs is given by $d(i,j)$.

	Pair (i,j)	d(i,j) (Å)	J_{ij}^{xx} (meV)	J_{ij}^{yy} (meV)	J_{ij}^{zz} (meV)	D_{ij}^{x} (meV)	D_{ij}^{y} (meV)	D_{ij}^{z} (meV)	$\lvert D\rvert$ (meV)	$\lvert D\rvert/\langle J_{ij}\rangle$	m (μ_B)	T_c (K)	MGS ($T = 0$ K)
CrS_2											2.5	106	$s-$AFM ($in-xy$)
	(1,2)	3.220	3.82	3.81	3.75	0	0	0	0	0			
	(1,3)	3.333	3.24	3.23	3.19	0	0	0	0	0			
$CrSe_2$											2.7	20	$z-$AFM ($t-xyz$)
	(1,2)	3.303	9.93	9.92	9.83	0	0	0	0	0			
	(1,3)	3.400	-0.25	-0.19	-0.11	0	0	0	0	0			
	(2,3)	3.457	-0.24	-0.20	-0.11	0	0	0	0	0			
$CrTe_2$											3.2	133	FM ($in-xy$)
	(1,2)	3.213	1.56	0.90	1.74	0	0	0	0	0			
	(1,3)	3.999	-6.92	-6.38	-7.16	0	0	0	0	0			
CrSSe											3.0	250	FM ($t-xz$)
	(1,2)	3.186	-8.11	-7.82	-8.12	-0.33	-0.11	-0.06	0.35	0.04			
	(1,3)	3.264	-9.15	-9.74	-9.75	-0.02	0.19	0.10	0.21	0.02			
	(2,3)	3.398	-0.34	-0.33	-0.32	0.09	0.08	0.23	0.26	0.77			
	(3,4)	3.457	-11.22	-11.26	-11.24	0.02	0.00	0.38	0.38	0.03			
	(3,5)	3.460	-9.33	-9.35	-9.31	0.02	0.124	-0.03	0.13	0.01			
	(3,6)	3.484	-6.76	-6.77	-6.76	0.06	0.14	-0.01	0.15	0.02			
	(4,7)	3.499	-8.11	-8.13	-8.12	-0.33	-0.12	-0.05	0.35	0.04			
CrSTe											2.9	299	FM ($t-yz$)
	(1,2)	3.435	-7.81	-8.14	-7.86	-0.41	0.00	0.39	0.56	0.07			
	(1,3)	3.488	-12.62	-12.60	-12.85	-0.48	0.38	-0.23	0.65	0.05			
CrSeTe											3.0	209	FM ($in-xy$)
	(1,2)	3.504	-3.93	-4.21	-4.16	-1.26	-0.1	0.13	1.27	0.31			
	(1,3)	3.508	-13.11	-13.09	-13.17	-0.34	1.01	1.46	1.80	0.14			
	(1,4)	3.526	-8.27	-8.24	-7.11	0.68	0.96	-0.38	1.24	0.16			
	(1,8)	3.534	-7.94	-8.01	-7.91	0.68	-1.09	-0.36	1.33	0.17			
	(2,3)	3.537	-8.83	-7.40	-7.30	0.28	1.28	-0.55	1.42	0.18			
	(2,4)	3.552	-8.56	-8.54	-8.61	-0.53	0.53	0.58	0.95	0.11			
	(2,5)	3.576	-1.72	-1.97	-1.83	-0.92	0.20	0.1	0.95	0.51			
	(3,4)	3.590	-3.28	-3.53	-3.43	-1.46	0.14	0.28	1.49	0.44			
	(3,5)	3.604	-8.61	-8.53	-8.73	0.71	1.04	-0.49	1.35	0.16			
	(3,6)	3.610	-8.81	-8.92	-8.72	-0.29	1.01	0.47	1.15	0.13			
	(4,6)	3.621	-11.41	-11.43	-11.39	0.34	0.98	-0.83	1.33	0.12			
	(4,7)	3.624	-1.57	-1.85	-1.67	-0.87	-0.16	0.04	0.89	0.52			

B. Magnetic properties

Next we discuss the magnetic properties of the considered monolayers in greater detail. Since the considered 2D materials exhibit distorted structures, even the pristine dichalcogenide ones, the magnetic interactions are expected to vary depending on the chosen pair of Cr atoms. Therefore, every unique pair is determined based on the interatomic distance (down to 10^{-3} Å precision). Then the corresponding magnetic exchange interaction matrix is calculated, using the 4-state methodology. In Table III we list the obtained exchange parameters for all the calculated Cr pairs (i,j), labeled according to Fig. 3. In order to isolate the considered pair from its repeating image in the periodic system, we used the supercell approach (the pairs aligned parallel to y-axis were calculated using 1×2 supercell, otherwise 2×1 supercell was used). The interaction matrices of the unlisted pairs were determined by rotation operation on that of ob-

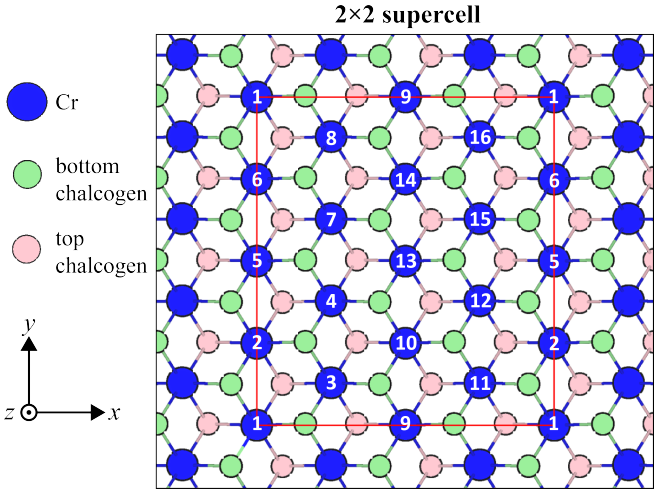

FIG. 3: Schematic depiction of the considered supercell in the magnetic exchange interactions calculations, with indices of the atoms shown. 1×2 supercell is used to calculate the exchange interaction of the pairs parallel to the y-axis, otherwise the 2×1 supercell is used.

tained pairs with the same distance.

In monolayer CrS_2, the magnetic interaction matrices of two distinct pairs of Cr atoms (cf. Table III and Fig. 3) are sufficient to define the magnetic interaction throughout the material. We found that the diagonal elements of the interaction matrices, which correspond to symmetric-isotropic interaction, for both Cr pairs have anti-ferromagnetic (AFM) nature, where in-plane components are slightly larger than the out-of-plane ones. That feature is visualized in the temperature-dependent coordinate-decomposed magnetization in Fig. 4. Cr-1 and Cr-2 exhibit parallel magnetic moments, and they are anti-parallel to the aligned magnetic moments of Cr-3 and Cr-4. The phase transition from paramagnetic to anti-ferromagnetic order occurs at $T_c = 106$ K and the system ends up in-plane stripy(s)-AFM configuration at $T = 0$ K, as shown in Fig. 4. This is consistent with the previous reports based on DFT analysis[51]. Monolayer $CrSe_2$ has three uniquely different pairs, where one exhibits strong FM interaction along a zig-zag chain of Cr, while the other two pairs have weak AFM interaction. Together, such interactions foster a zig-zag ($z-$)AFM configuration below the (rather low) T_c of 20 K. At $T = 0$, the magnetic moments are slightly tilted, with somewhat larger tilt in the y-direction. In the last considered pristine dichalcogenide, $CrTe_2$, two unique pairs are found sufficient to describe magnetic interactions; while one of them shows strong FM interaction, the other exhibits weak AFM interaction. Since the number of pairs equivalent to the FM one is larger than that of (weak) AFM pairs, the FM long-range order is established below $T_c = 133$ K, and system exhibits in-plane FM configuration at T=0 K. In preceding work, Lv *et al.* found FM and AFM orderings in $CrTe_2$ and $CrSe_2$ monolayers respectively, based on a first-principles study. They also reported that magnetic properties can be tuned by strain, i.e. strain induces a switch from FM (AFM) to AFM (FM) state in a $CrTe_2$ ($CrSe_2$) monolayer[54]. Furthermore, Xiuxian *et al.* reported a FM ground-state for $CrTe_2$ monolayer[55]. Monolayer $CrTe_2$ was recently experimentally grown on bilayer graphene by molecular beam epitaxy (MBE) and was reported to be FM with a T_c of ~ 200 K[31]. Our results show agreement with these studies. Conversely, Xian *et al.* observed a stable AFM order[30] in a $CrTe_2$ monolayer grown on a SiC supported bilayer graphene. These discrepancies between experimental results regarding the magnetic ground state of $CrTe_2$ could be attributed to different interfacial strain and/or substrate temperature.

Regarding the magnetic properties of the Janus layers, we commence with CrSSe. As mentioned in the structural analysis, CrSSe is visually the most intrinsically deformed monolayer among the considered ones. As a consequence, 7 unique Cr-pairs need to be considered to properly describe magnetic interactions throughout the monolayer. All those pairs were found to exhibit FM interaction, varying from very weak (~ -0.3 meV) to very strong (~ -11 meV). This set of exchange interactions results in T_c of 250 K of the FM state, as shown in Fig. 4. FM interaction at all pairs and the resultant FM magnetic state at $T = 0$ K from the LLG simulations were not expected, since we found the $s-$AFM state as the lowest-energy configuration in the DFT scheme. In order to test this peculiar result, we return to the DFT routine and considered FM configuration on the structure obtained for $s-$AFM order, which indeed delivered lower energy than what we had previously, and lower energy than the FM state with nearly perfect 1T structure (which was found to be unstable). Fig. 5 shows the three lowest-energy states, for three different magnetic orders, and three different degrees of deformation, once again demonstrating a strong interplay between magnetic order and the structural symmetry in this material.

The other two studied Janus monolayers, CrSTe and CrSeTe, exhibit FM order with T_c of 299 and 209 K, respectively. The magnetic configurations at $T = 0$ K for both layers, as obtained in LLG simulations, are slightly different to those found in the DFT scheme, yet consistent. CrSTe exhibits slight tilting of the moments from the out-plane direction, and CrSeTe has small additional out-of-plane component compared to the preceding DFT analysis.

Further regarding the Janus monolayers, a strong DMI is expected to arise since the inversion symmetry that Cr-pairs see is broken between the top and bottom chalcogens, and also due to the distortion of the octahedral coordination. Our calculated values of DMI magnitude $|D|$ and its ratio to the average isotropic exchange $|D|/\langle J_{ij}\rangle$ of the given Cr-pair (i, j) are listed in Table III. In the Janus CrSSe, which is the most intrinsically distorted among the studied monolayers, exhibits weak $|D|$, in average ≈ 0.26 meV. This is just 3% of the average isotropic exchange interaction of -7.62 meV. For in-

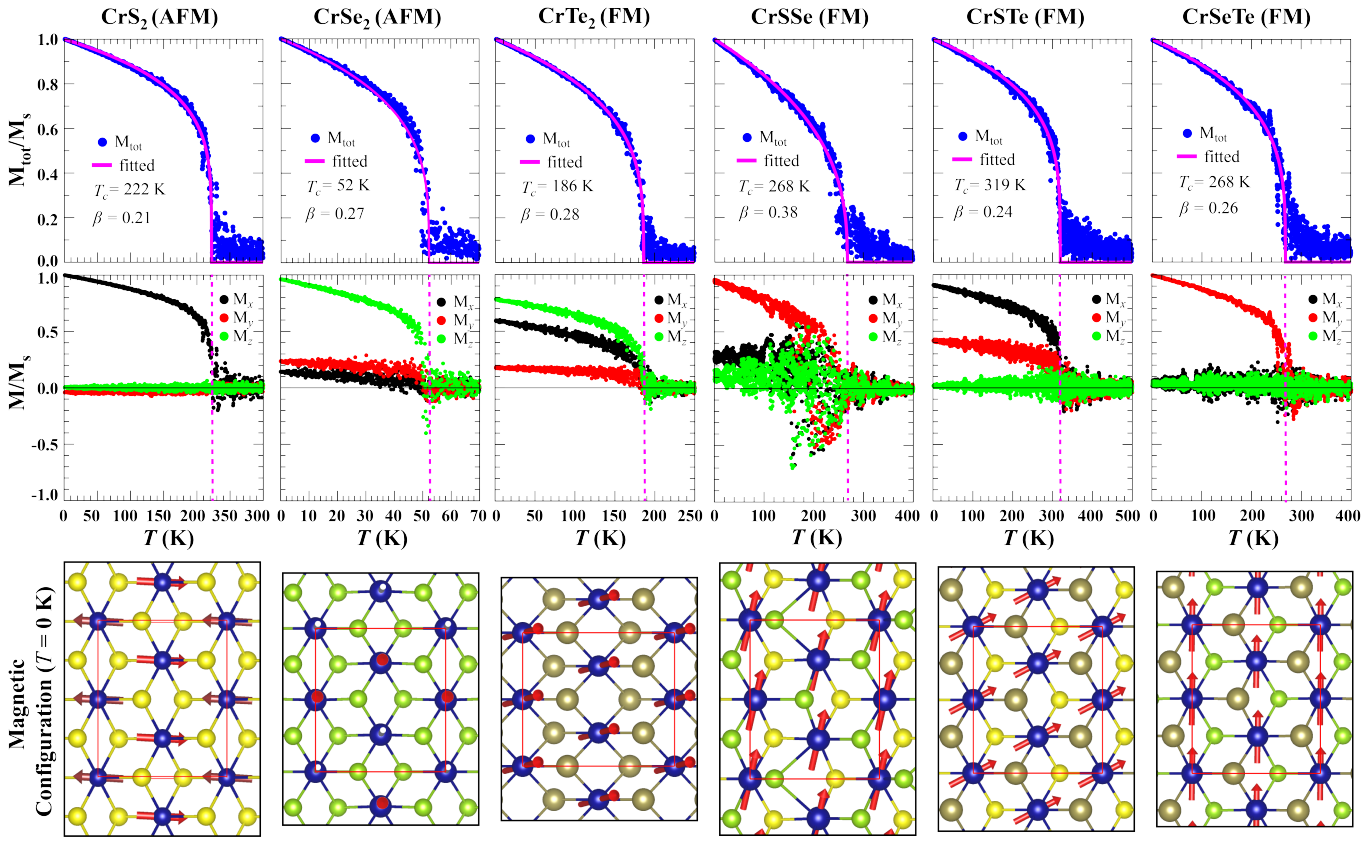

FIG. 4: Temperature-dependent normalized magnetization obtained via LLG simulation, based on the magnetic interaction parameters given in Table III, for the ground-state magnetic order shown in the bottom most panel. In the case of a FM ground state, the upper and lower top panels show the total and the coordinate-decomposed magnetization, respectively. In the case of an AFM order, those panels the magnetization of one of the FM sub-configurations is plotted, since the total magnetization is zero.

stance, $|D|/\langle J_{ij}\rangle$ is found to be 77% for the $(2,3)$ pair of CrSSe. However, $\langle J_{ij}\rangle$ is also weak on that pair, therefore there is no significance of that large ratio in the magnetic properties. Janus CrSTe monolayer exhibits stronger average $|D|$ of 0.61 meV as compared to CrSSe, but the $\langle J_{ij}\rangle$ is also stronger, resulting in still small $|D|/\langle J_{ij}\rangle$ ratio of about 6 % in average. The strongest DMI is found in Janus CrSeTe monolayer, having amplitude of 1.26 meV in average, which corresponds to 24.5% of -5.15 meV of the average isotropic exchange. This large ratio stands out when compared to those of the $Cr(I,Br)_3$ (27%) and $Cr(I,Cl)_3$ (29.40 %) Janus monolayers[23], since the corresponding exchange interactions are relatively small in those materials, and suggests formation of non-collinear spin textures in the ground state. Our results for CrSSe and CrSeTe agree with those of a recent theoretical study of 2D Janus chromium dichalcogenides under strain[58]. The latter study showed that the CrSTe monolayer has high T_c of 295 K and an out-of-plane magnetic anisotropy, while CrSeTe has large DMI which favors the formation of chiral Néel domain walls (DWs). They also found that the DW in CrSeTe can be tuned into skyrmion states with an external magnetic field and strain[58].

IV. CONCLUSIONS

In summary, we have detailed the structural, electronic, vibrational and magnetic properties of 2D Janus CrXY (X,Y=S,Se,Te, with X≠Y) monolayer materials and compared them to those of 2D pristine CrX_2 monolayers, using relativistic density-functional calculations, including DFT+U correction, the four-state energy mapping methodology (4SM) to extract all relevant magnetic interactions, and the atomistic spin relaxation to obtain the ground-state spin textures and the critical temperature of the long-range magnetic order. In the Janus CrXY monolayers, where inversion symmetry is broken between different surface chalcogens, the different electronegativities and atomic numbers between chalcogen atoms (X and Y) induce not only changes in the structural parameters compared to those of the pristine 1T-CrX_2, but also the nondegenerated d states of Cr deviate from those in the ideally octahedral crystal field. As a consequence, the type of the dominant p(chalcogen)-d(Cr) interaction will strongly depend on the geometric organization of the chalcogen atoms around the Cr atom, which in turn influences the electronic structure

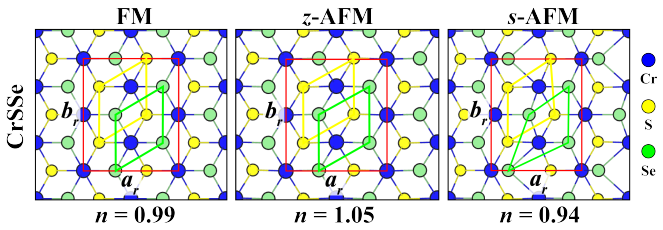

FIG. 5: Top view of the optimized structure of CrSSe for three different magnetic orders: FM, $z-$AFM, and $s-$AFM. The yellow (bottom S) and green (top Se) show the ordering. While $z-$AFM is in nearly perfect 1T form, $s-$AFM case presents the most distorted structure (with buckled Cr layer shown in 1), which exhibits the lowest energy.

and magnetic properties of each considered 2D Janus CrXY monolayer.

Concerning the favorable magnetic order, we find that monolayer CrS_2 and $CrSe_2$ exhibit $s-$AFM and $z-$AFM order with critical temperature T_c of 106 and 20 K, respectively. However, $CrTe_2$ exhibits in-plane FM order, up to T_c of 133 K. As expected there is no DMI found in these pristine pristinedichalcogenide monolayers, due to preserved inversion symmetry. The Janus CrSSe is a FM material, with T_c of 250 K. It should be noted that CrSSe exhibits significantly distorted structure, both in-plane and out-of-plane (i.e. buckled chromium mid-layer), very strongly coupled to the magnetic order. Janus CrSTe and CrSeTe monolayers are also in FM order, with T_c of 299 and 209 K, respectively. Although all structures of the Janus monolayers are significantly distorted, DMI is particularly strong only for monolayer CrSeTe, being 1.26 meV in average, which corresponds to 24.5% of the average isotropic exchange and suggests possibility of formation of stable non-collinear spin textures with non-zero topological charge (such as magnetic skyrmions).

The very strong coupling between the spin textures and the lattice structure found in these Cr-based (pristine and Janus) monolayer dichalcogenides, together with their versatile electronic properties (metal or semiconducting), high critical temperature of their magnetic order, as well as the coupling between the magnetic and electronic degrees of freedom (DMI and polarization) with every present symmetry breaking, suggest these materials for further experimental exploration and use in spintronic, sensing and piezo-magneto-electric applications.

Acknowledgments

This work was supported by the Special Research Funds of the University of Antwerp (BOF-UA), the Research Foundation-Flanders (FWO), and by Universidad del Norte (UniNorte). The calculations were performed in part using the facilities of the Flemish Supercomputer Center (VSC), funded by the FWO and the Flemish Government – department EWI.

* Electronic address: milorad.milosevic@uantwerpen.be

[1] N. D. Mermin and H. Wagner, Physical Review Letters **17**, 1133 (1966).
[2] P. C. Hohenberg, Physical Review **158**, 383 (1967).
[3] W. Cong, Z. Tang, X. Zhao, and J. Chu, Scientific Reports **5**, 9361 (2015).
[4] A. González-García, W. López-Pérez, R. González-Hernández, C. Bacaksiz, D. Šabani, M. Milošević, and F. Peeters, Journal of Physics: Condensed Matter **33**, 145803 (2021).
[5] P. Ong, N. Kioussis, P. K. Amiri, J. Alzate, K. Wang, G. P. Carman, J. Hu, and R. Wu, Physical Review B **89**, 094422 (2014).
[6] E. Torun, H. Sahin, C. Bacaksiz, R. T. Senger, and F. M. Peeters, Physical Review B **92**, 104407 (2015).
[7] B. Huang, G. Clark, E. Navarro-Moratalla, D. R. Klein, R. Cheng, K. L. Seyler, D. Zhong, E. Schmidgall, M. A. McGuire, D. H. Cobden, et al., Nature **546**, 270 (2017).
[8] C. Gong, L. Li, Z. Li, H. Ji, A. Stern, Y. Xia, T. Cao, W. Bao, C. Wang, Y. Wang, et al., Nature **546**, 265 (2017).
[9] L. Chen, C. Mao, J.-H. Chung, M. B. Stone, A. I. Kolesnikov, X. Wang, N. Murai, B. Gao, O. Delaire, and P. Dai, Nature communications **13**, 4037 (2022).
[10] I. Dzyaloshinsky, Journal of Physics and Chemistry of Solids **4**, 241 (1958).
[11] T. Moriya, Physical Review **120**, 91 (1960).
[12] M. Hervé, B. Dupé, R. Lopes, M. Böttcher, M. D. Martins, T. Balashov, L. Gerhard, J. Sinova, and W. Wulfhekel, Nature Communications **9**, 1 (2018).
[13] M. Yagmurcukardes, Y. Qin, S. Ozen, M. Sayyad, F. M. Peeters, S. Tongay, and H. Sahin, Applied Physics Reviews **7**, 011311 (2020).
[14] L. Zhang, Z. Yang, T. Gong, R. Pan, H. Wang, Z. Guo, H. Zhang, and X. Fu, Journal of Materials Chemistry A **8**, 8813 (2020).
[15] C. Xia, W. Xiong, J. Du, T. Wang, Y. Peng, and J. Li, Physical Review B **98**, 165424 (2018).
[16] R. Li, Y. Cheng, and W. Huang, Small **14**, 1802091 (2018).
[17] V. Van Thanh, N. D. Van, R. Saito, N. T. Hung, et al., Applied Surface Science **526**, 146730 (2020).
[18] A.-Y. Lu, H. Zhu, J. Xiao, C.-P. Chuu, Y. Han, M.-H. Chiu, C.-C. Cheng, C.-W. Yang, K.-H. Wei, Y. Yang, et al., Nature nanotechnology **12**, 744 (2017).
[19] J. Zhang, S. Jia, I. Kholmanov, L. Dong, D. Er, W. Chen, H. Guo, Z. Jin, V. B. Shenoy, L. Shi, et al., ACS nano **11**, 8192 (2017).
[20] Z. Guan, N. Luo, S. Ni, and S. Hu, Materials Advances **1**, 244 (2020).
[21] J. Liang, W. Wang, H. Du, A. Hallal, K. Garcia, M. Chshiev, A. Fert, and H. Yang, Physical Review B **101**, 184401 (2020).
[22] J. Yuan, Y. Yang, Y. Cai, Y. Wu, Y. Chen, X. Yan, L. Shen, et al., Physical Review B **101**, 094420 (2020).
[23] C. Xu, J. Feng, S. Prokhorenko, Y. Nahas, H. Xiang, and

L. Bellaiche, Physical Review B **101**, 060404 (2020).
[24] Y. Hou, F. Xue, L. Qiu, Z. Wang, and R. Wu, npj Computational Materials **8**, 120 (2022).
[25] M. R. Habib, S. Wang, W. Wang, H. Xiao, S. M. Obaidulla, A. Gayen, Y. Khan, H. Chen, and M. Xu, Nanoscale **11**, 20123 (2019).
[26] A. Shivayogimath, J. D. Thomsen, D. Mackenzie, M. Geisler, R.-M. Stan, A. J. Holt, M. Bianchi, A. Crovetto, P. R. Whelan, A. Carvalho, et al., Nature communications **10**, 1 (2019).
[27] J. Sugiyama, H. Nozaki, I. Umegaki, T. Uyama, K. Miwa, J. H. Brewer, S. Kobayashi, C. Michioka, H. Ueda, and K. Yoshimura, Physical Review B **94**, 014408 (2016).
[28] D. C. Freitas, M. Nunez, P. Strobel, A. Sulpice, R. Weht, A. A. Aligia, and M. Nunez-Regueiro, Physical Review B **87**, 014420 (2013).
[29] D. C. Freitas, R. Weht, A. Sulpice, G. Remenyi, P. Strobel, F. Gay, J. Marcus, and M. Núñez-Regueiro, Journal of Physics: Condensed Matter **27**, 176002 (2015).
[30] J.-J. Xian, C. Wang, J.-H. Nie, R. Li, M. Han, J. Lin, W.-H. Zhang, Z.-Y. Liu, Z.-M. Zhang, M.-P. Miao, et al., Nature Communications **13**, 1 (2022).
[31] X. Zhang, Q. Lu, W. Liu, W. Niu, J. Sun, J. Cook, M. Vaninger, P. F. Miceli, D. J. Singh, S.-W. Lian, et al., Nature communications **12**, 1 (2021).
[32] J. He and S. Li, Computational Materials Science **152**, 151 (2018).
[33] P. Hohenberg and W. Kohn, Physical Review **136**, B864 (1964).
[34] W. Kohn and L. J. Sham, Physical Review **140**, A1133 (1965).
[35] J. P. Perdew, K. Burke, and M. Ernzerhof, Physical Review Letters **77**, 3865 (1996).
[36] P. E. Blöchl, Physical Review B **50**, 17953 (1994).
[37] G. Kresse and D. Joubert, Physical Review B **59**, 1758 (1999).
[38] G. Kresse and J. Furthmüller, Computational Materials Science **6**, 15 (1996).
[39] G. Kresse and J. Furthmüller, Physical Review B **54**, 11169 (1996).
[40] S. Grimme, Journal of Computational Chemistry **27**, 1787 (2006).
[41] V. I. Anisimov, J. Zaanen, and O. K. Andersen, Physical Review B **44**, 943 (1991).
[42] M. Cococcioni and S. De Gironcoli, Physical Review B **71**, 035105 (2005).
[43] A. Togo and I. Tanaka, Scripta Materialia **108**, 1 (2015).
[44] G. Kresse, J. Furthmüller, and J. Hafner, EPL (Europhysics Letters) **32**, 729 (1995).
[45] K. Parlinski, Z. Li, and Y. Kawazoe, Physical Review Letters **78**, 4063 (1997).
[46] H. Xiang, C. Lee, H.-J. Koo, X. Gong, and M.-H. Whangbo, Dalton Transactions **42**, 823 (2013).
[47] D. Šabani, C. Bacaksiz, and M. Milošević, Physical Review B **102**, 014457 (2020).
[48] G. P. Müller, M. Hoffmann, C. Dißelkamp, D. Schürhoff, S. Mavros, M. Sallermann, N. S. Kiselev, H. Jónsson, and S. Blügel, Physical Review B **99**, 224414 (2019).
[49] M. J. Varjovi and E. Durgun, Physical Review Materials **5**, 104001 (2021).
[50] Y. Cheng, Z. Zhu, M. Tahir, and U. Schwingenschlögl, EPL (Europhysics Letters) **102**, 57001 (2013).
[51] C. Wang, X. Zhou, Y. Pan, J. Qiao, X. Kong, C.-C. Kaun, and W. Ji, Physical Review B **97**, 245409 (2018).
[52] S. Lebègue, T. Björkman, M. Klintenberg, R. M. Nieminen, and O. Eriksson, Physical Review X **3**, 031002 (2013).
[53] K. Chen, J. Deng, Y. Yan, Q. Shi, T. Chang, X. Ding, J. Sun, S. Yang, and J. Z. Liu, npj Computational Materials **7**, 1 (2021).
[54] H. Lv, W. Lu, D. Shao, Y. Liu, and Y. Sun, Physical Review B **92**, 214419 (2015).
[55] X. Yang, X. Zhou, W. Feng, and Y. Yao, Physical Review B **103**, 024436 (2021).
[56] J. Jiao, N. Miao, Z. Li, Y. Gan, J. Zhou, and Z. Sun, The Journal of Physical Chemistry Letters **10**, 3922 (2019).
[57] B. Zhou, Q. Zhao, Z. Liu, X. Shen, X. Ye, J. Shi, Z. Liao, W. Wang, Z. Hu, H.-J. Lin, et al., NPG Asia Materials **12**, 1 (2020).
[58] Q. Cui, J. Liang, Z. Shao, P. Cui, and H. Yang, Physical Review B **102**, 094425 (2020).